Published in final edited form as:
*Acta Biomater*. 2012 July ; 8(7): 2476–2482. doi:10.1016/j.actbio.2012.04.011.

# Amphiphilic Protein Micelles for Targeted In Vivo Imaging

**Wookhyun Kim**[†], **Colin Brady**[‡], and **Elliot L. Chaikof**[†,*]

[†]Department of Surgery, Beth Israel Deaconess Medical Center, Harvard Medical School, and the Wyss Institute of Biologically Inspired Engineering of Harvard University, Boston, MA, USA

[‡]Department of Surgery, Emory University, Atlanta, GA, USA

## Abstract

A variety of polymeric nanoparticles have been developed for bioimaging applications. In this study, we report use of a 50 nm recombinant protein nanoparticle with a multivalent surface as a vehicle for functionalization with a model imaging agent. Multiple fluorescent probes were covalently conjugated to surface amines of crosslinked amphiphilic elastin-mimetic protein micelles using N- hydroxysuccinimide ester chemistry. In vivo fluorescence imaging confirmed that protein micelles selectively accumulated at sites of angioplasty induced vessel wall injury presumably via an enhanced permeability and retention (EPR) effect. This investigation demonstrates the potential of amphiphilic protein micelles to be used as a vehicle for selective imaging of sites associated with disrupted or leaky endothelium.

### Keywords

polypeptides; protein micelles; conjugation; vascular permeability; bioimaging

## 1. Introduction

Fluorescent nanoparticles have been used to localize and assess the extent of a variety of pathological processes [1–4]. In this regard, both encapsulation and covalent conjugation of fluorophores have been used to generate fluorescent nanoparticle [5–7]. Even without surface targeting groups, nanoparticles selectively accumulate at sites of increased vascular permeability often associated with tumor microcirculation or inflammatory processes via an enhanced permeability and retention (EPR) effect [2,8–10].

Recent strategies to create probes for biomedical imaging have included organic and inorganic nanoparticles, quantum dots (QD), liposomes, proteins, and viral particles [2,3,11–16]. Although each approach has unique advantages, none has proven ideal due to concerns related toxicity, biostability, and bioavailability. Among these probes, QDs are the most interesting class of fluorescent probes for bioimaging because of their brightness, photostability and narrow and tunable emission spectrum. In addition to QDs, magnetic nanoparticles such as iron oxides have been used as contrast enhancing agent for magnetic resonance imaging (MRI) and coupled with fluorescent probes for both MRI and



[*]Address correspondence to: Elliot L. Chaikof, M.D., Ph.D., Department of Surgery, Beth Israel Deaconess Medical Center, 110 Francis St, Suite 9F, Boston, MA 02115, Tel: (617) 632-9581, echaikof@bidmc.harvard.edu.

fluorescence imaging. However, under physiological conditions, QDs and magnetic nanoparticles are not soluble and tend to aggregate. In addition, Cd, Te, Se or Pb found in QDs are cytotoxic [17]. Protein-based nanoparticles may have several advantages over other imaging agents including limited toxicity and enhanced biocompatibility, particularly for elastin-based micro- or nanoparticles [18–20]. Significantly, such particles display inherent flexibility for functionalization with bioactive molecules either chemically or genetically [21–24]. For example, Simnick et al. have recently reported the generation of elastin-like diblock copolymers that have been engineered with an RGDS peptide sequence at the N terminus and one cysteine residue at the C terminus that can be chemically conjugated to a fluorescent probe containing maleimide [24]. Our group has recently developed recombinant amphiphilic diblock polypeptides (ADP) based on elastin-mimetic sequences that consist of a N-terminal hydrophilic block and a C-terminal hydrophobic block containing glutamic acid and tyrosine residues, respectively. We demonstrated that these polypeptides formed 50 nm diameter thermally responsive micellar nanoparticles that exhibited a spherical core-shell structure. By introducing multiple cysteine residues between the amphiphilic blocks, it was possible to obtain stable protein micelles through disulfide bond formation at the core-shell interface [25,26].

In this study, we describe the surface functionalization of elastin-mimetic protein (EMP) micelles via chemical conjugation and the potential to use these particles for in vivo bioimaging. Each diblock polypeptide possesses a single free amine at the N terminus, which is displayed on the surface of the protein micelle due to self-assembly of C-terminal hydrophobic blocks that occurs above their inverse transition temperature. Thus, we anticipated that functionalizing elastin-mimetic protein micelles with fluorescent dyes via an NHS ester linker would generate protein nanoparticles with enhanced fluorescent intensity.

Interventional vascular procedures, such as balloon angioplasty and stent implantation lead to endothelial injury, which may contribute to subsequent restenosis and arterial occlusion. An effective noninvasive modality to image the extent of endothelial denudation after procedures does not exist. To evaluate the utility of fluorescently-labeled protein micelles, we studied their use in detecting discrete sites of vascular wall injury. Balloon injury results in the loss of the endothelium with significant local enhancement of vessel wall permeability. The EPR effect after angioplasty has been demonstrated using Evans blue staining, which associates with serum albumin, as well as with hydrophobic drug-conjugated nanoparticles [2,27,28]. We hypothesized that accumulation of fluorescent EMP micelles could be used as a non-invasive marker for enhanced permeability and retention that characterizes vascular wall injury. In this investigation, EMP micelles were evaluated in a rat aortic balloon injury model with micelle uptake visualized by an in vivo fluorescent imaging system. To our knowledge, this is the first report in which protein nanoparticles were used to image sites of vessel wall injury via an EPR effect.

## 2. Materials and Methods

### 2.1. Materials

All chemical reagents were purchased from Fisher Scientific, Inc. (Pittsburgh, PA) unless otherwise noted. Texas red®-X succinimidyl ester or fluorescein succinimidyl ester were purchased from invitrogen (Eugene, Oregon). TALON metal affinity resin was purchased from BD Biosciences, Inc. Methods used to produce the diblock genes encoding amphiphilic diblock polypeptide (ADP) derived from elastin-mimetic sequences, $[(VPGVG)(VPGEG)(VPGVG)(VPGEG)(VPGVG)]_{10}$ for hydrophilic N-block and $[(IPGVG)_2VPGYG(IPGVG)_2]_{15}$ for hydrophobic C-block, have been described previously [24]. Expression of the diblock synthetic genes with N-terminal his-tag sequence in *E. coli* expression strain, BL21(DE3), afforded recombinant amphiphilic diblock polypeptide in a

high yield (50 mg/L culture) when 1 mM isopropyl β-D-1-thiogalactopyranoside was added. Purification was performed by immobilized metal affinity chromatography (IMAC) from the cell lysate. Aqueous solutions of ADP were prepared from lyophilized specimens of the purified protein polymer that was dissolved at the appropriate concentration in distilled, deionized water or PBS at 4°C. The purified protein polymer has been characterized by SDS-PAGE (Sodium Dodecyl Sulfate-Polyacrylamide Gel Electrophoresis), MALDI mass, amino acid compositional analysis, and $^{1}$H NMR [25].

## 2.2. Methods

**2.2.1. Preparation and characterization of elastin-mimetic micelles—**Stock solutions of ADP were prepared by dissolving the solid protein (1 mg/mL) with cold water. For preparation of protein micelles, the protein solution was diluted to 0.3 mg/mL with PBS and kept on ice for one hour. The tube containing diluted solution was subsequently moved to a 25 °C water bath and incubated for 30 min. A micelle suspension was stored under constant agitation at room temperature for 2 weeks and changes in micelle size and size distribution were monitored by DLS (DynaPro, Protein Solutions).

**2.2.2. Labeling protein micelles with fluorescent dye and characterization—**N-terminal amines of elastin-mimetic micelles were modified with an amine-reactive fluorescent probe. Solutions of the protein micelles in 1 mL of PBS were prepared at 25 °C. A total of 10 μL of Texas red®-X succinimidyl ester or fluorescein succinimidyl ester dissolved in DMSO at a concentration of 10 mM was added dropwise to ADP solutions. The reaction mixture was stirred at room temperature in the dark overnight and then dialyzed against PBS for 72 hrs to remove unreacted dyes. For synthesis of dual dye-labeled micelles, fluorecein succinimidyl ester was added to Texas Red-micelle conjugate dispersion and the reaction mixture was stirred at room temperature in the dark overnight. Non-reacted dyes were removed by dialysis.

Fluorescently labeled protein micelles were analyzed by UV spectroscopy, fluorescence spectroscopy, DLS, and gel filtration and visualized by illumination on a standard UV light box. UV-vis spectra were recorded on a Cary UV-visible spectrophotometer (Varian Inc.) in 1 cm quartz cuvette. Degree of labeling was determined from the absorbance of maximum peak of dyes (Fluorescein 494 nm and Texas Red 593 nm) using an extinction coefficient (68,000 for Fluorescein and 80,000 $M^{-1}cm^{-1}$ for Texas Red, respectively) relative to concentration of diblock polypeptide. Fluorescence spectra of fluorophore-conjugated micelles were obtained using PC1 photon counting spectrofluorometer (ISS inc.). Fluorescein was excited at 494 nm and the emission spectra were recorded from 500 to 600 nm. Texas Red was excited at 594 nm and the emission spectra were recorded from 595 to 700 nm. Size and polydispersity of dye-micelle conjugates were analyzed by dynamic light scattering using a DynaPro (Protein Solutions) at 25 and 37 °C. Sample solutions were filtered through a 0.45 μm nylon syringe filter prior to DLS measurements. DLS measurements were carried out at a fixed scattering angle of 90°. The molecular weight of the protein micelles was estimated from the hydrodynamic radius using the standard curve of model proteins. The number of a single diblock polypeptide associated in one micelle, was determined by $MW_{micelle}/MW_{polypeptide}$. Zeta potential was determined from three measurements using DLS (Malvern Zetasizer, zen3600). Gel filtration for size exclusion chromatography (Hi-Prep 16/60, Sephacryl-S100, High resolution) was performed to analyze homogeneity of protein micelles. The column was pre-equilibrated with PBS buffer and protein micelles were eluted with a flow rate of 0.6 mL/min.

**2.2.3. Rat Balloon injury and Evans blue staining—**Balloon injury was performed to a discrete 10 mm segment of rat thoracic aorta with a 2F Fogarty catheter (10 – 12 week old

Wistar Rats, 300 – 400 g, Jackson Laboratory, Bar Harbor, Maine). Induction of anesthesia was performed in a Plexiglas chamber with isoflurane gas anesthetic (5 % inhalant to effect). Anesthesia was maintained by isoflurane inhalational anesthetic at 1.5 – 2 % continuous flow. All animals had free access to standard water and chow and received care and monitoring in compliance with established guidelines (i.e. per the Institutional Animal Care and Use Committee).

Five animals were assessed at each time point after balloon injury (1 h, 7, 14, 21 days). At the time of sacrifice a jugular venous cut down was performed and Evans blue solution (1 mL, 5 mg/mL) was injected into the venous circulation. One hour after Evans blue injection, the laparotomy site was reopened and the thoracic contents were surgically exposed. Saline irrigation was performed via direct access of the left ventricle until liver congestion, color change and intestinal edema was noted. The IVC was transected to allow for euthanasia via exsanguination. Sharp dissection was used to release the aorta from its surrounding tissues along its length, extending from the aortic arch to the bifurcation. The aortic segment was harvested and analyzed by gross visualization. Injury zones stained dark blue due to the uptake of Evans Blue dye. Image processing software, Image J (NIH, USA) was used to determine the surface area of the blue stained injury zone. This process was repeated to assess the change in injury zone surface area over time.

**2.2.4. Balloon injury of rat aorta and fluorescent imaging—**Balloon injury was performed to a discrete 10 mm segment of rat thoracic aorta with a 2F Fogarty catheter (Wistar Rats, 300 – 350 g, Jackson Laboratory, Bar Harbor, Maine). All animals had free access to standard water and chow, receiving care and monitoring in compliance with guidelines established by the Institutional Animal Care and Use Committee. Immediately following injury, TR-micelles (1 mL, 0.5 mg/mL micellar solution in PBS) were injected intravenously. The conjugate was allowed to circulate for 24 hours prior to harvest. Harvested samples were imaged enface on an Olympus OV100 fluorescent imaging system. Filters were chosen to encompass the excitation/emissions wavelengths of Texas Red 595/615 nm, respectively. System parameters (i.e. exposure time, maximum/minimum intensities, and focal length) were kept constant for each acquisition, and images were acquired at 6x magnification. With the use of the OV100 software package, heat maps of fluorescent images were generated and exported as .tiffs for further analysis.

We created a novel image analysis program utilizing MatLab (The Mathworks Inc.) to quantify the heat maps. The program allowed for pixel quantification corresponding to each of the eight-intensity bars defining the heat map. Each colorimetric bar of the heat map is associated with a fixed mean fluorescent intensity value. The percent surface area of each of these colors within the injured region was plotted against mean fluorescent intensity to obtain a histrographic representation of the data. Additionally, the eight intensity bars of the heat map were grouped into high (top three bars), medium (middle two bars) and low (bottom three bars) as another means of representing the data with respect to percent surface area of the stent.

## 3. Results and Discussion

### 3.1. Conjugation of fluorescent dye to surface of protein micelle

The surface of amphiphilic EMP micelles can be functionalized with a variety of biomolecules, such as fluorescent probes or specific targeting ligands through chemical or recombinant approaches. For chemical modification, we employed amine-reactive molecules because only a single amino group is available for conjugation in the polypeptide sequence. Formation of spherical micelles with a core-shell structure generated nanoparticles with a multivalent aminated surfaces due to the presence of terminal amines in

the hydrophilic block. Thus, bifunctional chemical linkers containing NHS ester facilitate the derivatization of surface protein nanoparticles with bioactive molecules.

To examine the feasibility of N-terminal conjugation, fluorescent dyes with an NHS ester moiety, NHS-Texas red and NHS-Fluorescein, were used to modify the surface of amphiphilic EMP micelles (Figure 1). Briefly, Texas red succinimidyl ester (NHS-Texas red) was added to a micellar solution in PBS buffer to generate Texas Red derivatized protein micelles (TR-micelle). The labeling reaction was incubated at room temperature overnight and unreacted dye subsequently removed through dialysis against PBS buffer for 72 hr (Figure 2A left and 2B).

### 3.2. Characterization of fluorescently labeled protein micelle

We characterized the protein micelles by dynamic light scattering (DLS). The number of diblock polypeptides associated into one protein micelle was determined from molecular weight of protein micelle [24]. The estimated molecular weight of the spherical protein micelles was 6,035 kDa as determined by DLS. Given that the molecular weight of a single diblock polypeptide chain was 56.9 kDa, a single micelle was formed from the assembly of approximately 106 diblock polypeptide chains with a corresponding number of free amines displayed on the surface. The degree of labeling, as measured by UV-vis spectroscopy, revealed a ratio of dye molecules per mole of diblock copolypeptide of 0.5 – 0.6 consistent with estimated 50 – 60 dye molecules per protein micelle, which was also confirmed by fluorescence spectroscopy using a standard curve based on free dye.

Conjugation of multiple fluorophores to a given protein molecule, such as an antibody, can cause significant reduction of fluorescence intensity by quenching interactions between closely located dyes. However, large protein particles, such as virus nanoparticles have been labeled with multiple fluorescent dyes and the dye-virus conjugates generate highly fluorescent particles without fluorescence quenching [15]. Similarly, EMP micelles doped with a number of fluorescent dyes have no observable fluorescence quenching, even after prolonged storage, probably due to the flexible hydrophilic chains and long intermolecular distances between fluorophores.

Labeling of EMP micelles with fluorophores was confirmed by UV-vis spectroscopy and fluorescence spectroscopy (Figure 2D,E and Figure S2). We also examined labeling micelles with both dyes by sequential conjugation of TR-micelles with NHS Fluorescein. UV spectroscopy of TR/FL-micelle conjugates exhibited two absorption maxima at 494 and 593 nm that are characteristic for each fluorophore, respectively (Figure 2D). Dual dye labeling suggests that EMP micelles could serve as multimodal protein nanoparticles with the incorporation of appropriate imaging agents.

The fluorescently labeled protein micelles were further analyzed by size exclusion chromatography using gel filtration (Figure 2C). The presence of tyrosine residues in hydrophobic block facilitated detection of eluted protein micelles. TR- and FL-labeled protein micelles displayed elution times identical to those of non-labeled micelles. As illustrated by DLS and gel filtration profiles, dye conjugation did not dissociate micelle structure or substantially alter size.

After conjugation with a fluorescent probe, size and stability of fluorescently labeled EMP micelles were monitored by DLS (Figure 3, Table 1). TR-micelles were stable when stored at room temperature in PBS with constant shaking for 2 weeks. Under physiologic conditions, micelle stability remains a critical determinant of the suitability of a given formulation. As a surrogate measure of biostability, DLS was used to assess micelle dimensions in the presence of 10% fetal bovine serum (FBS) at 37 °C. A small increase in

polydispersity and micelle size was noted after a 1 hr incubation period. The zeta potential was measured to study the variation in surface charge. The outer shell of EMP micelles contains glutamic acid residues in the hydrophilic block and an aminated surface. The zeta potential of unlabeled EMP micelles was negative due to highly carboxylated shell (−13 mV). After conjugation of the N-terminal amino group with a fluorescent probe, the zeta potential decreased due to a reduction in number of protonated amino groups on micelle surface (−18 mV). Therefore, the zeta potential together with UV and fluorescence spectroscopy suggested the presence of fluorescent probes on the micelle surface and improved stability of the fluorescently-labeled micelles at neutral pH.

### 3.3. Balloon injury of rat aorta and fluorescent imaging

Interventional vascular procedures are commonly used for the treatment of atherosclerotic occlusive disease. However, such intervention inevitably leads to damage of the vessel wall. Removal of the endothelium by balloon injury results in exposure of collagen to blood, platelet deposition and may be followed by proliferation and migration of vascular smooth muscle cells. In particular, the risk of restenosis and arterial occlusion remains high after treatment of extensive complex lesions that are characteristic of lower extremity peripheral arterial disease. One of the interesting biologic properties of the vascular endothelium is to mediate vascular permeability. Previous studies have shown that even marginal disruption of this architecture can significantly enhance vascular wall permeability [27, 28]. Given the inevitable endothelial injury during endoluminal vascular interventions, the capacity to detect the site of vessel wall injury may provide a rational approach to monitor the integrity of endothelium as an initial marker of vascular wall injury. However, there has been no reliable modality for identifying the extent of endothelial denudation after an interventional procedure.

Vascular targeting strategies to detect vessel wall injury include ligand-based targeting and EPR-based targeting. Ligand-based targeting strategy is considered as effective, but difficult to generate. Among targeting ligands to vascular injury, glycoprotein VI (GPVI) is known as a collagen receptor, which is expressed on platelets and plays a critical role in the activation and aggregation of platelets at the site of injury. A fusion protein of GPVI and a human C-terminal Fc fragment exhibited selective binding to collagen and the site of vessel wall injury in vivo [29, 30]. It has been recently reported that the use of FITC-glycoprotein VI (GPVI)-Fc (a human Fc fragment) conjugate facilitated the fluorescence imaging of vascular lesions via targeting to collagen exposed to blood flow after endothelial denudation [30]. In contrast, enhanced vascular permeability-based targeting involves the selective uptake of EMP micelles at the site of vessel wall injury.

Prior to in vivo application of the EMP micelles, we first confirmed that balloon injury of the rat thoracic aorta lead to a reproducible model of vessel wall injury. Endothelial denudation over a 10 mm length with an associated increase in vascular permeability was identified by Evans blue staining (Figure 4). Injury zone of thoracic aorta was stained as blue by Evans blue dye while uninjured zone was not stained or only pale blue. Serial evaluation of the injury site by Evans Blue analysis revealed that the time to achieve 50% healing ($t_{50}$) was 8.1 days (Figure S3). Evans blue staining confirmed the existence of an EPR effects, consistent with prior reports [2,27].

The biodegradability of EMP micelles is a critical factor for in vivo imaging and its biocompatibility. For *in vivo* applications, micelles should be stable during circulation to effectively target the site of vessel wall injury but then undergo degradation. Liu *et al.* have determined the *in vitro* degradation rate after incubation with serum and *in vivo* degradation rate of $^{14}$C-labeled elastin-like polypeptides (ELP) after intravenous injection, which were 2.49% and 2.46% per day, respectively [31].

The capacity of protein micelles to selectively penetrate the injury site was assessed after IV administration of 0.5 mg of Texas red-labeled micelles. TR-micelle conjugates were injected in the immediate post-operative period and imaging performed after a 24 hr circulation time. Significantly, fluorescence imaging demonstrated that micelle uptake correlated with the extent of endothelial denudation and could be used to quantitate regions of increased micelle deposition in the injured vessel wall (Figure 5A–D). In contrast, micelle uptake was not observed in normal, uninjured aorta (Figure 5E,F).

## 4. Conclusions

In conclusion, the present study demonstrates the feasibility of multivalent attachment of fluorophores to amphiphilic EMP micelles with targeting to sites of vessel wall injury. Elastin-mimetic polypeptides have advantages over conventional polymers including minimal toxicity and good biocompatibility. The surface of EMP micelles was covalently modified with N-hydroxysuccinimide ester modified-fluorescent dyes via formation of an amide linkage without substantial fluorescent quenching. We expect that multivalent surface conjugation with near-infrared fluorescence probe (NIRF) or positron emitting agents would further facilitate non-invasve in vivo imaging. Moreover, we believe that multivalent display of targeting ligands including specific cell adhesive peptides or antibodies would further enhance selective particle targeting to distinct cell-surface receptors.

## Supplementary Material

Refer to Web version on PubMed Central for supplementary material.

## Acknowledgments

This work was supported by the NIH and the Juvenile Diabetes Research Foundation. Use of Malvern Zetasizer was supported by the Wyss Institute of Biologically Inspired Engineering of Harvard.

## References

1. Peer D, Karp JM, Hong S, Farokhzad OC, Margalit R, Langer R. Nanocarriers as an emerging platform for cancer therapy. Nat Nanotechnol. 2007; 2 (12):751–60. [PubMed: 18654426]
2. Nakanishi T, Fukushima S, Okamoto K, Suzuki M, Matsumura Y, Yokoyama M, Okano T, Sakurai Y, Kataoka K. Development of the polymer micelle carrier system for doxorubicin. J Controlled Release. 2001; 74 (1–3):295–302.
3. Adams ML, Lavasanifar A, Kwon GS. Amphiphilic block copolymers for drug delivery. J Pharm Sci. 2003; 92 (7):1343–55. [PubMed: 12820139]
4. Shi H, He X, Wang K, Yuan Y, Deng K, Chen J, Tan W. Rhodamine B isothiocyanate doped silica-coated fluorescent nanoparticles (RBITC-DSFNPs)-based bioprobes conjugated to Annexin V for apoptosis detection and imaging. Nanomedicine. 2007; 3 (4):266–72. [PubMed: 17988954]
5. Sandanaraj BS, Gremlich HU, Kneuer R, Dawson J, Wacha S. Fluorescent nanoprobes as a biomarker for increased vascular permeability: Implications in diagnosis and treatment of cancer and inflammation. Bioconjugate Chem. 2010; 21 (1):93–101.
6. Tanisaka H, Kizaka-Kondoh S, Makino A, Tanaka S, Hiraoka M, Kimura S. Near-infrared fluorescent labeled peptosome for application to cancer imaging. Bioconjugate Chem. 2008; 19 (1): 109–17.
7. Peters D, Kastantin M, Kotamraju VR, Karmali PP, Gujraty K, Tirrell M, Ruoslahti E. Targeting atherosclerosis by using modular, multifunctional micelles. Proc Natl Acad Sci USA. 2009; 106 (24):9815–9. [PubMed: 19487682]
8. Maeda H, Wu J, Sawa T, Matsumura Y, Hori K. Tumor vascular permeability and the EPR effect in macromolecular therapeutics: a review. J Controlled Release. 2000; 65 (1–2):271–84.

9. Lukyanov AN, Hartner WC, Torchilin VP. Increased accumulation of PEG-PE micelles in the area of experimental myocardial infarction in rabbits. J Controlled Release. 2004; 94 (1):187–93.
10. Torchilin VP. Micellar nanocarriers: pharmaceutical perspectives. Pharm Res. 2007; 24 (1):1–16. [PubMed: 17109211]
11. Yang CS, Chang CH, Tsai PJ, Chen WY, Tseng FG, Lo LW. Nanoparticle-based in vivo investigation on blood-brain barrier permeability following ischemia and reperfusion. Anal Chem. 2004; 76 (15):4465–71. [PubMed: 15283589]
12. Josephson L, Kircher MF, Mahmood U, Tang Y, Weissleder R. Near-infrared fluorescent nanoparticles as combined MR/optical imaging probes. Bioconjugate Chem. 2002; 13 (3):554–60.
13. Torchilin VP. Recent advances with liposomes as pharmaceutical carriers. Nat Rev Drug Discovery. 2005; 4 (2):145–60.
14. Mulder WJM, Castermans K, van Beijnum JR, Oude Egbrink MG, Chin PTK, Fayad ZA, Lowik CWGM, Kaijzel EL, Que I, Storm G, Strijkers GJ, Griffioen AW, Nicolay K. Molecular imaging of tumor angiogenesis using alphavbeta3-integrin targeted multim odal quantum dots. Angiogenesis. 2009; 12 (1):17–24. [PubMed: 19067197]
15. Lewis JD, Destito G, Zijlstra A, Gonzalez MJ, Quigley JP, Manchester M, Stuhlmann H. Viral nanoparticles as tools for intravital vascular imaging. Nat Med. 2006; 12 (3):354–60. [PubMed: 16501571]
16. Mulder WJ, Strijkers GJ, Habets JW, Bleeker EJ, van der Schaft DW, Storm G, Koning GA, Griffioen AW, Nicolay K. MR molecular imaging and fluorescence microscopy for identification of activated tumor endothelium using a bimodal lipidic nanoparticle. FASEB J. 2005; 19 (14): 2008–10. [PubMed: 16204353]
17. Kirchner C, Liedl T, Kudera S, Pellegrino T, Javier AM, Gaub HE, Stolzle S, Fertig N, Parak WJ. Cytotoxicity of colloidal CdSe and CdSe/ZnS nanoparticles. Nano Lett. 2005; 5 (2):331–8. [PubMed: 15794621]
18. Urry DW, Parker TM, Reid MC, Gowda DC. Biocompatibility of the bioelastic materials, poly(GVGVP) and its gamma-irradiation cross-linked matrix - Summary of generic biological test-results. J Bioact Compat Pol. 1991; 6 (3):263–82.
19. Rincon AC, Molina-Martinez IT, de Las Heras B, Alonso M, Bailez C, Rodriguez-Cabello JC, Herrero-Vanrell R. Biocompatibility of elastin-like polymer poly(VPAVG) microparticles: in vitro and in vivo studies. J Biomed Mater Res Part A. 2006; 78 (2):343–51.
20. Sallach RE, Cui W, Wen J, Martinez A, Conticello VP, Chaikof EL. Elastin-mimetic protein polymers capable of physical and chemical crosslinking. Biomaterials. 2009; 30 (3):409–22. [PubMed: 18954902]
21. Raucher D, Chilkoti A. Enhanced uptake of a thermally responsive polypeptide by tumor cells in response to its hyperthermia-mediated phase transition. Cancer Res. 2001; 61 (19):7163–70. [PubMed: 11585750]
22. Dreher MR, Simnick AJ, Fischer K, Smith RJ, Patel A, Schmidt M, Chilkoti A. Temperature triggered self-assembly of polypeptides into multivalent spherical micelles. J Am Chem Soc. 2008; 130 (2):687–94. [PubMed: 18085778]
23. MacKay JA, Chen M, McDaniel JR, Liu W, Simnick AJ, Chilkoti A. Self-assembling chimeric polypeptide-doxorubicin conjugate nanoparticles that abolish tumours after a single injection. Nat Mater. 2009; 8 (12):993–9. [PubMed: 19898461]
24. Simnick AJ, Valencia CA, Liu R, Chilkoti A. Morphing low-affinity ligands into high-avidity nanoparticles by thermally triggered self-assembly of a genetically encoded polymer. ACS Nano. 2010; 4 (4):2217–27. [PubMed: 20334355]
25. Kim W, Thevenot J, Ibarboure E, Lecommandoux S, Chaikof EL. Self-assembly of thermally responsive amphiphilic diblock copolypeptides into spherical micellar nanoparticles. Angew Chem Int Ed. 2010; 49 (25):4257–60.
26. Kim W, Xiao J, Chaikof EL. Recombinant amphiphilic protein micelles for drug delivery. Langmuir. 2011; 27 (23):14329–34. [PubMed: 21973265]
27. Uwatoku T, Shimokawa H, Abe K, Matsumoto Y, Hattori T, Oi K, Matsuda T, Kataoka K, Takeshita A. Application of nanoparticle technology for the prevention of restenosis after balloon injury in rats. Circ Res. 2003; 92 (7):e62–9. [PubMed: 12663484]

28. Weidinger FF, McLenachan JM, Cybulsky MI, Gordon JB, Rennke HG, Hollenberg NK, Fallon JT, Ganz P, Cooke JP. Persistent dysfunction of regenerated endothelium after balloon angioplasty of rabbit iliac artery. Circulation. 1990; 81 (5):1667–79. [PubMed: 2139594]

29. Gawaz M, Konrad I, Hauser AI, Sauer S, Li Z, Wester H-J, Bengel FM, Schwaiger M, Schömig A, Massberg S, Haubner R. Non-invasive imaging of glycoprotein VI binding to injured arterial lesions. Thromb Haemost. 2005; 93:910–3. [PubMed: 15886808]

30. Bigalke B, Pohlmeyer I, Schonberger T, Griessinger CM, Ungerer M, Botnar RM, Pichler BJ, Gawaz M. Imaging of injured and atherosclerotic arteries in mice using fluorescence-labeled glycoprotein VI-Fc. Eur J Radiol. 2011; 79:e63–9. [PubMed: 21497471]

31. Liu W, Dreher MR, Furgeson DY, Peixoto KV, Yuan H, Zalutsky MR, Chilkoti A. Tumor accumulation, degradation and pharmacokinetics of elastin-like polypeptides in nude mice. J Controlled Release. 2006; 116:170–8.

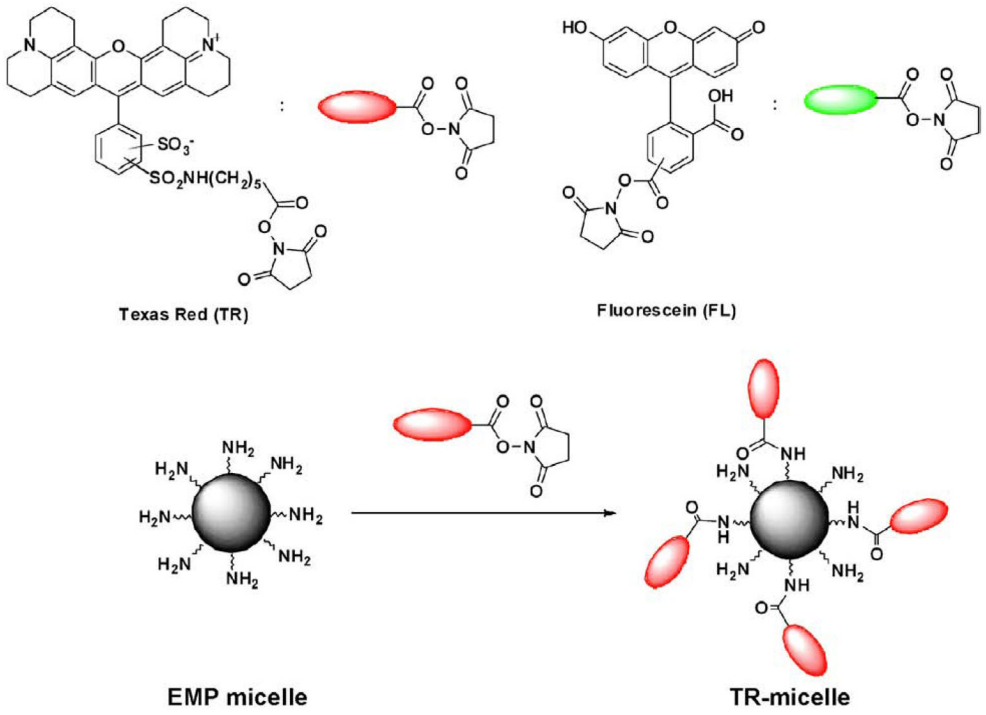


**Figure 1.**
Labeling of N-terminal amines of elastin-mimetic protein micelles with amine-reactive fluorescent probes, Texas red (TR) and Fluorescein (FL) NHS esters.

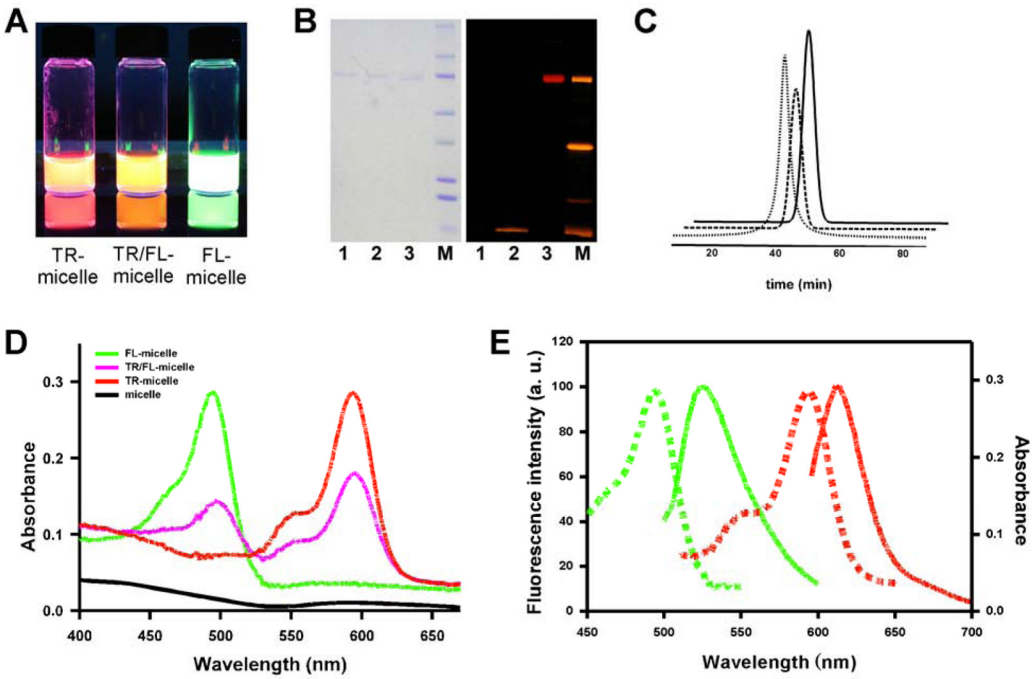


**Figure 2.**

(**A**) UV illumination of aqueous dispersion of TR-micelle, TR/FL-micelle and FL-micelle conjugates, respectively. (**B**) SDS-PAGE analysis and UV illumination to detect TR-micelle conjugate. 1, unlabeled protein micelles; 2, mixture of micelles and non-NHS fluorophore (Rhodamine B); 3, Texas red-micelle conjugate (TR-micelle); M, molecular weight standard. (**C**) Size exclusion chromatographic analysis of un-labeled micelle (dotted), TR-micelle (dashed) and FL-micelle conjugate (solid). (**D**) UV-visible spectra of un-labeled protein micelle (black), TR-micelle (red), FL-micelle (green) and TR/FL-micelle conjugate (pink). (**E**) Fluorescence spectra (solid lines) of FL-micelle (green) and TR-micelle (red).

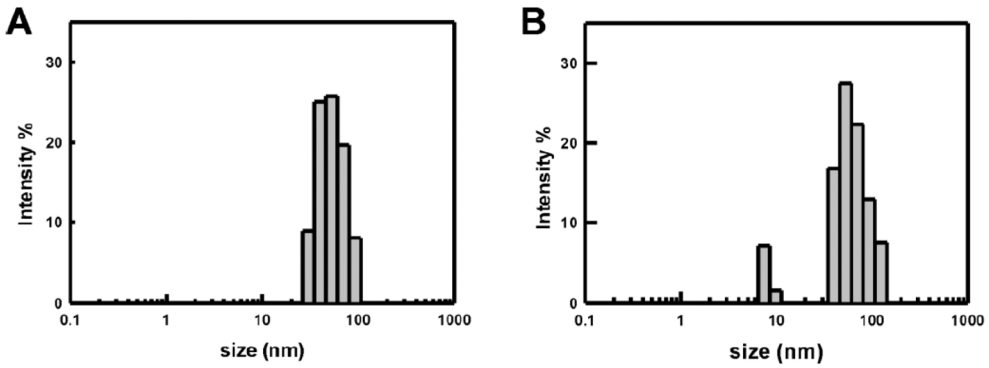


**Figure 3.**
Dynamic light scattering (DLS) measurements of (**A**) TR-micelle and (**B**) TR-micelle/10% FBS at 37 °C.

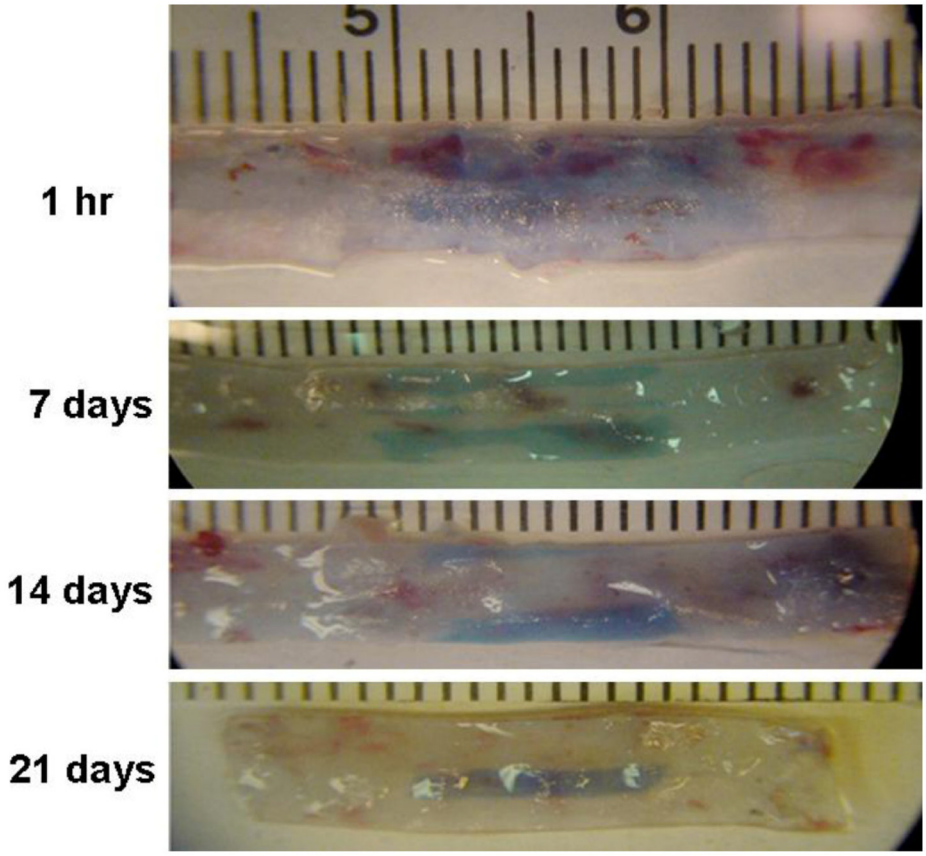


**Figure 4.**

Balloon injury of rat aorta visualized by Evans blue staining. Five animals were assessed at each time point after balloon injury (1 h, 7, 14, 21 days). At the time of sacrifice Evans blue solution (1 mL, 5 mg/mL) was injected into the venous circulation. One hour after dye injection, saline irrigation was performed via direct access of the left ventricle. The aortic segment was harvested and the injury zone of thoracic aorta was visualized as dark blue color with non-injured regions indicated by an absence of Evans blue staining.

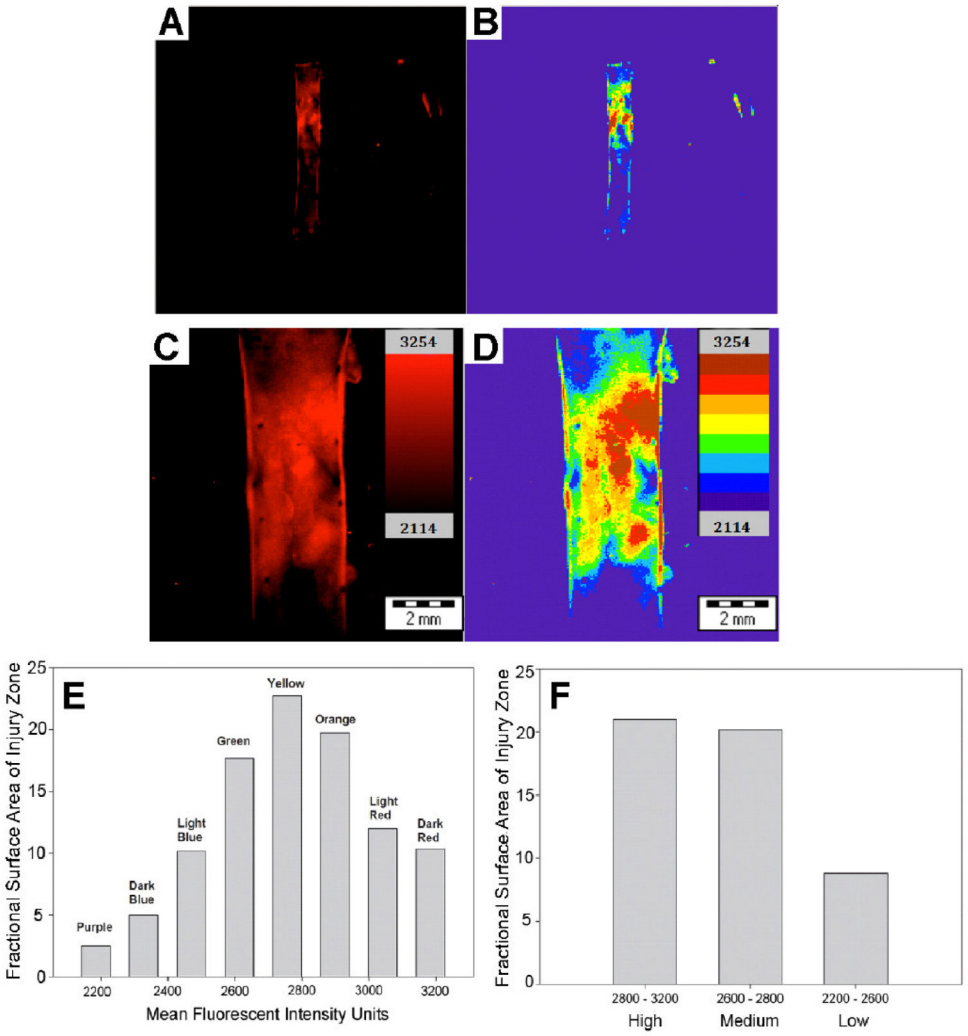


**Figure 5.**

Rat aortic balloon injury model imaged with TR-micelles. Injury zone defined by Evans Blue correlates with penetration of Texas Red labeled-micelles, which were administered IV and allowed to circulate for 24 hrs. The sample was imaged in the OV100 at low (**A**, **B**) and high magnification (6x magnification) (**C, D**). Fluorescence uptake was not observed in the uninjured vessel wall. Micelle uptake can be quantitated as a colormetric modular heat map (**B, D**) with the spatial distribution of fluorescence intensity levels presented as histogram plots (**E, F**).

## Table 1

Summary of size and polydispersity for unlabeled and TR-labeled protein micelles

| | Size (nm) | PDI [a] |
|---|---|---|
| micelle | 49.2 | 0.17 |
| micelle + BSA[b] | 70.0[e] | 0.12 |
| micelle + BSA + TCEP[c] | 172.2[e] | 0.01 |
| TR-micelle + FBS[d] | 73.2 | 0.28 |
| TR-micelle conjugate (t=0) | 59.0 | 0.24 |
| TR-micelle conjugate (t=2 weeks, PBS, 23°C) | 65.3 | 0.59 |

[a] polydispersity index (PDI);

[b] Bovine serum albumin (BSA) (3 $mgmL^{-1}$);

[c] 1 mM tris(2-carboxyethyl)phosphine (TCEP);

[d] 10% fetal bovine serum (FBS);

[e] Reference 25.